Tensile strength of calcite/HMWM and silica/HMWM interfaces: A Molecular Dynamics analysis

K. Ji[a], C. Arson[a,*]

[a]*School of Civil and Environmental Engineering, Georgia Institute of Technology, USA*

Abstract

The mechanical behavior of interfaces between high molecular weight methacrylate (HMWM) and concrete minerals (calcite and silica) is investigated from a Molecular Dynamics (MD) perspective. MD simulations of pullout tests shows that interfaces debond at the surface of contact between HMWM and the mineral substrate, and that the interfacial strength decreases in the presence of moisture, under low strain rate, or at high temperature. Silica/HMWM interfaces are stronger than the calcite/HMWM interfaces. Additionally, the work of separation is mostly done by van der Waals forces, in agreement with previous studies. We use published experimental data at low strain rate along with our MD results at high strain rate to calibrate Richeton's model and Johnson-Cook model. We show that, if more experimental results were available for validation, MD results could be extrapolated to predict the tensile modulus of HMWM at low strain rate and the HMWM/mineral interfacial strength for a broad range of temperatures and strain rates. The sensitivity analysis of the model confirms that HMWM

*Corresponding author.
E-mail address: chloe.arson@ce.gatech.edu
Phone: 404-385-0143

should be applied on dry surfaces and in concrete exposed to lower temperatures. Additionally, MD results suggest that HMWM is more likely to last in concrete with high silica contents than in concrete with high calcite contents.
Keywords: molecular dynamics, concrete, High Molecular Weight Methacrylate (HMWM), interface strength, van der Waals forces, strain rate

1. Introduction

Sustainability and durability of concrete structures are major concerns in both developed and developing countries. For instance, in the United States, the most destructive cause of early deterioration of steel-reinforced concrete bridges is steel chloride-ion-induced corrosion [1]. To ensure the sustainability of concrete structures, it is critical to delay the travel time of chloride ions to the steel reinforcements as much as possible. Local application of sealants is viewed as a good way to repair shrinkage cracks in the early stages of crack propagation. An extensive literature review of deck sealants and crack sealants was reported in [2], concluding that epoxies and High-Molecular-Weight-Methacrylate (HMWM) were the best-performing sealants: epoxies allow recovering flexural strength but can only be injected in larger cracks, while HMWM can efficiently penetrate narrow cracks and reduce the permeability of concrete. These conclusions are supported by recent studies investigating the sealing potential of HMWM for concrete airfield pavements [3]. HMWM is recommended to repair cracks of various widths [4, 5, 6] and is used to clog cracks and to restore the structural bond strength of concrete in bridge decks.

Poromechanical models of concrete allow predicting shrinkage cracks and the resulting mechanical and transport properties [7, 8, 9], but they were never applied to concrete repaired with sealants. Some researchers used the Finite Element Method (FEM) to simulate the mechanical behavior of concrete repaired by epoxy, but the model is purely mechanical and time-independent [10]. At the atomistic scale, Molecular Dynamics (MD) can be used to measure the cohesive strength of the interface between a metallic or ceramic substrate and epoxy [11, 12, 13], and to predict the moisture transport processes in epoxy materials [14]. MD allows simulating damage initiation and propagation in a broad range of interface systems. The stress-strain response and yield strength of atom-scale interfaces can be obtained. MD also allows calculating the glass transition temperature and the density of a variery of polymers.

MD was first used to study the dynamic behavior on a system of several hundred atoms [15]. Later, increased computational power and fundamental advances in chemistry allowed applying MD to solve problems of chemical engineering, bioengineering and physics. Due to the importance of intermolecular interactions between polymers and concrete minerals on interface adhesion [16], MD was used to understand the relationship between the mechanical properties and the chemical structure of the interfaces between polymers and metals and polymers and minerals [17, 18, 19, 20, 21, 22]. However, previous studies were mainly focused on certain epoxies such as Diglycidyl Ether of Bisphenol F (EPON-862) mixed with Diethyl toluene diamine (DETDA) and asphalt materials. For instance, MD allowed understanding the influence of the cutoff distance and of the stoichiometric

mixture on the behavior of EPON-862 and DETDA [23]. Li and Strachan studied the process of polymerization and crosslinking in polymers using the DREIDING force field, with Buckingham van der Waals interactions [24]: the mass density, glass transition temperature, thermal expansion coefficient and elastic modulus calculated numerically were in good agreement with experiments. Yang and collaborators [25] studied tensile deformation and failure mechanisms in epoxy/copper composite materials through large scale MD simulations, using the polymer consistent force field (PCFF). However, MD studies of sealant/concrete interfaces remain scarce.

In the present paper, we aim to understand the fundamental processes that govern the mechanical behavior of interfaces between HMWM and concrete minerals (calcite and silica) at atomistic scale, from an MD perspective. We first present our MD models of calcite, silica and HMWM in Section 2. Then, Section 3 explains the MD models of mineral/HMWM interfaces and presents the results of pullout tests that are simulated under different strain rates, temperatures and moisture conditions. Section 4 is a discussion that focuses on the effect of strain rate. We summarize our findings in Section 5.

2. Molecular models of the interface components

2.1. Principle of the Molecular Dynamics simulations

In order to build a model in MD, the molecular structure of the materials first has be optimized. Then, the boundary conditions are applied and the potential energy function is defined. In the simulation step, Newton's second law is used to calculate how forces affect the motions of atoms, as follows:

$$\boldsymbol{a}(t) = \frac{\boldsymbol{F}(t)}{m}, \quad \boldsymbol{F}(t) = \nabla U(\boldsymbol{x}(t), t) \tag{1}$$

where $\boldsymbol{F}(t)$ is the force exerted on an atom at time t, m is the mass of the atom, $\boldsymbol{a}(t)$ is the atom's acceleration at time t, and $\boldsymbol{x}(t)$ is the atom's position at time t. U is the potential energy function. To integrate the equations of motion, Verlet algorithm is employed, as follows:

$$x_i(t_0 + \Delta t) = 2x_i(t_0) - x_i(t_0 - \Delta t) + (\Delta t)^2 a_i(t_0) \tag{2}$$

where $x_i(t_0)$ is the position vector at t_0, $x_i(t_0 - \Delta t)$ is the position vector at $t_0 - \Delta t$ and $a(t_0)$ is the acceleration vector at time t_0. Atomic positions and velocities are updated iteratively, based on the knowledge of the initial positions and velocities, and based on the choice of the force field. The latter expresses the forces experienced by an atom given the positions of the other atoms. The choice of the force field function plays an important role in the calculation of the molecular system's potential energy, which is derived from numerous experimental datasets and approximations. Classically, the potential energy function E_t is composed of a bonding force field potential E_b and of non-bonding force field potential E_{nb}. In the present model, we use the DREIDING force field equation to account for interactions between atoms. The DREIDING potential energy was parametrized and validated for organic and inorganic materials, including polymers and crystals, and for various environmental conditions, including various moisture contents and a broad range of temperatures (100K-600K) [24, 26, 17, 27]. The total force field equation can be expressed as follows:

$$E_t = E_b + E_{nb} \tag{3}$$

$$E_b = \sum_b \frac{1}{2} K_b (b - b_0)^2 + \sum_\theta \frac{1}{2} K_\theta (\theta - \theta_0)^2 + \sum_\phi K_\phi \left(cos(\phi)\right)^i \tag{4}$$

$$E_{nb} = \sum_{i,j} 4\epsilon_{ij} \left[\left(\frac{r*_{ij}}{r_{ij}} \right)^{12} - \left(\frac{r*_{ij}}{r_{ij}} \right)^{6} \right], r_{ij} \leq r_c \quad (5)$$

In the second equation above, E_b is the covalent bond energy, in which K_b, K_θ, and K_ϕ are constants, and b_0 and θ_0 are respectively the equilibrium bond length and bond angle. b is the bond stretch, θ is the bond angle and ϕ is the dihedral torsion angle. In the third equation above, E_{nb} is Van der Waals energy (Lennard-Jones potential), in which r_{ij} is the distance between the ith and jth atoms with charges q_i and q_j. r_c is the cutoff distance, equal to 12Å in this study [24, 17]. For all the MD simulations presented in the following, we used LAMMPS and MAPS programs [28].

2.2. Molecular models of silica and calcite

Concrete mechanical properties are highly dependent on concrete structure and chemical composition, as highlighted in previous MD studies [19, 12]. The most abundant material components in concrete and cement are quartzite and limestone. Limestone aggregates mostly consist of calcium carbonate (calcite), and sand and granite are mainly made of quartzite (silica). Therefore, we modeled calcite and silica at the molecular scale to investigate the resistance of concrete/HMWM interfaces to debonding. Figure 1 shows the lattices of calcite and silica built in MD. For calcite, the dimensions of the lattice are $a = b = 4.990$Å, $c = 17.061$Å, $\alpha = \beta = 90°$ and $\gamma = 120°$. For silica, the dimensions of the lattice are $a = b = 4.913$Å, $c = 5.405$Å, $\alpha = \beta = 90°$ and $\gamma = 120°$.

2.3. Molecular model of HMWM

For the HMWM model, we first simulated the transition of HMWM to the glassy state, i.e. the process by which the hardener links with methyl

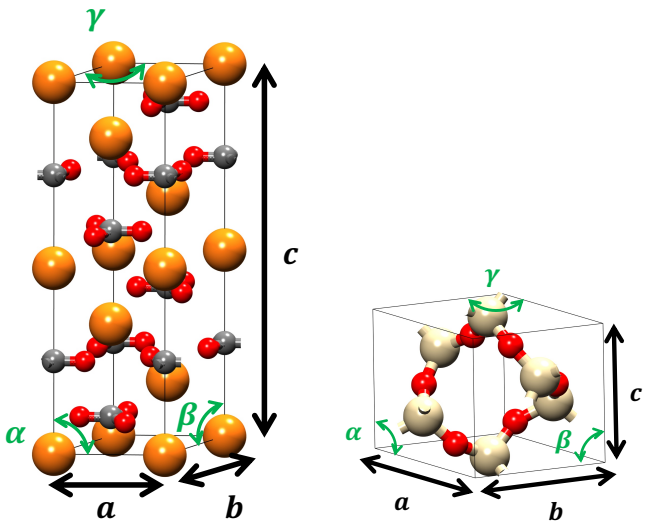

(a) Calcite (b) Silica

Figure 1: MD lattice models of representative concrete minerals. For calcite, calcium atoms are orange, carbon atoms are black and oxygen atoms are red. For quartz, silicon atoms are red, oxygen atoms are white. Calcite: $a = b = 4.990$Å, $c = 17.061$Å. Silica: $a = b = 4.913$Å, $c = 5.405$Å.

methacrylate (resin) towards a cured state, also known as cross-linking. Figure 2 illustrates the principle of the crosslinking reaction. We assumed that there was a free-radical polymerization of Methyl methacrylate (MMA). The radical initiator (cumene hydroperoxide) was decomposed to generate free radicals and to react with the MMA monomer [29]. The stoichiometric mixing ratio of methyl methacrylate and cumene hydroperoxide was 35:1, with a low initial density of $0.5g/cm^3$. We used a 3D periodic boundary condition. The positions of the atoms were iteratively adjusted so as to minimize the potential energy of the HMWM system. Then, following previous studies [26], the cross-linked system was subjected to an NVT ensemble simulation

(imposed number of particles, imposed volume and imposed temperature) under 600K, for $5 \times 10^{-11}s$ (10^5 timesteps of $\Delta t = 0.5fs$). The HMWM crosslinked structure obtained by MD is a relaxed polymer network (traction free condition), as shown in Figure 3.

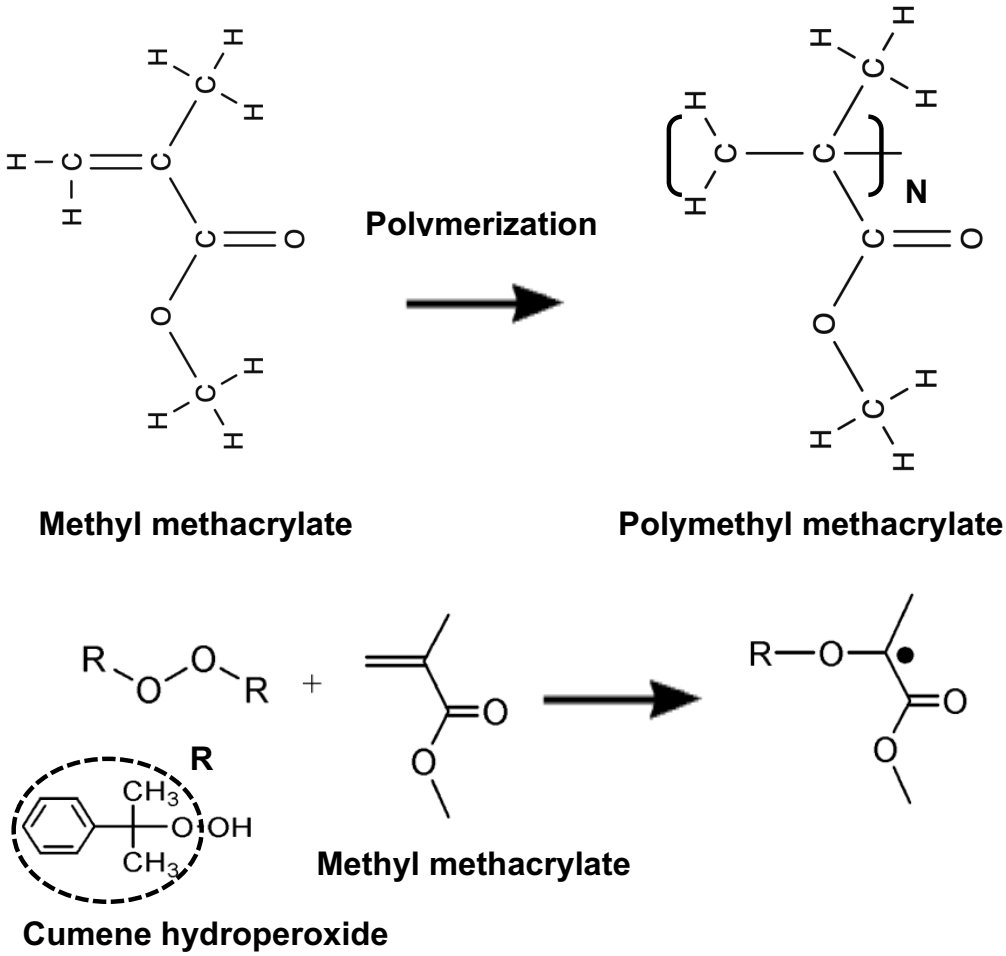

Figure 2: Schematic diagram of the chemical reactions involved in HMWM crosslinking.

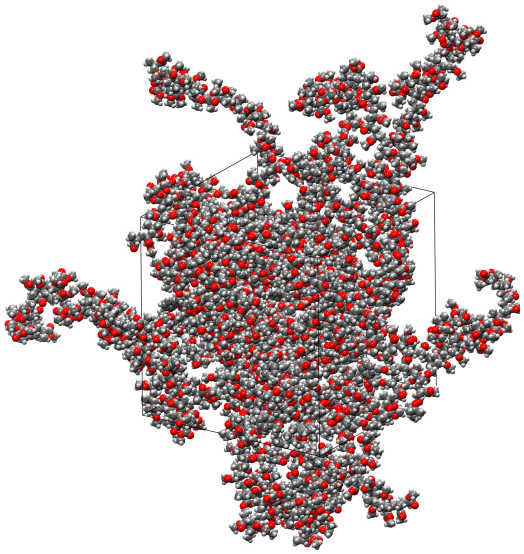

Figure 3: HMWM atomistic configuration after crosslinking. Carbon atoms are grey, oxygen atoms are red, hydrogen atoms are white.

2.4. Material properties of HMWM

After cross-linking and equilibration, we conducted a series of NPT simulations (imposed number of particles, pressure and temperature) to calibrate the following properties: epoxy glass transition temperature, mass density, Young's modulus, Poisson's ratio. To perform these simulations, we used the DREIDING Buckingham (X6) form for the van der Waals interactions, and Nose-Hoover temperature thermostat and pressure barostat. In order to achieve a relaxed amorphous polymer structure, a temperature of 600K was first maintained at atmospheric pressure for $2.5 \times 10^{-10}s$ (5×10^5 timesteps of $\Delta t = 0.5fs$). Then, we simulated annealing with the NPT ensemble, by decreasing the temperature from 600K to 300K, within $2.5 \times 10^{-10}s$ (5×10^5 timesteps of $\Delta t = 0.5fs$). Results obtained during the cooling stage are plotted in Figure 4. We employed a piecewise bilinear regression method in order to determine the glass transition temperature of HMWM, i.e. the temperature at the transition between the glassy and rubbery states of HMWM. The glass transition temperature predicted by MD is around 407K, which is conform to the glass transition temperature measured in published experiments [6]. Lastly, we simulated a relaxation test: a room temperature of 300K was applied for $2.5 \times 10^{-10}s$ (5×10^5 timesteps of $\Delta t = 0.5fs$). The calculated mass density at 300K was 1.053 g/cm^3, which is in good agreement with the experimental results presented in a previous study (0.995 to 1.068 g/cm^3) [6].

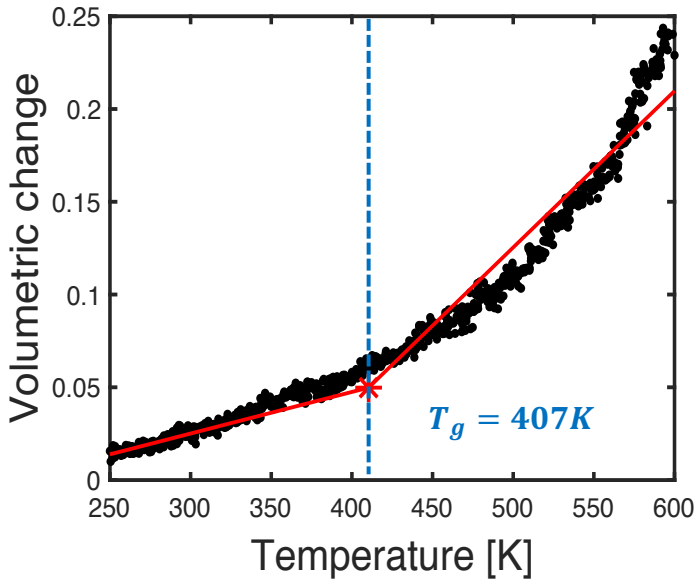

(a)

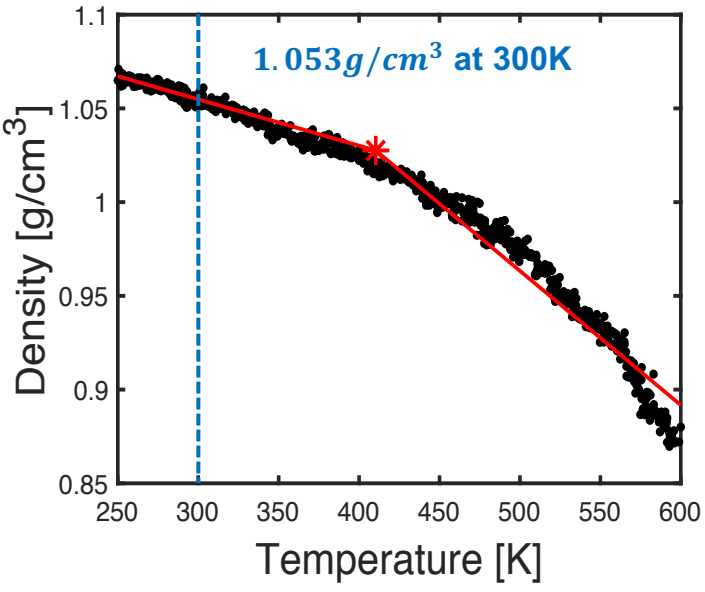

(b)

Figure 4: Simulation of an annealing test on cross-linked HMWM, at atmospheric pressure, decreasing the temperature from 600K to 300K. (a) Volumetric deformation vs. Temperature (b) Density vs. Temperature

To calculate the tensile modulus and the Poisson's ratio of the cross-linked epoxy, we simulated uniaxial tension tests under the atmospheric pressure, at a temperature of $300K$. The cross-linked epoxy model constructed with MAPS was first imported into LAMMPS. A uniaxial strain was uniformly applied at the top and at the bottom of the cross-linked HMWM model (called "box" in the following). We first simulated uniaxial tension at a strain rate of 5 x 10^8 s^{-1}, following previous work [24]. Figure 5 shows the simulated stress versus strain relationship. For strains in the range 5-8 %, the tensile modulus and the Poisson's ratio of the cross-linked HMWM are found to be in the range of 2.076-2.7 GPa and 0.3-0.35, respectively. Published experimental data on HMWM mechanical properties were obtained by subjecting specimens to quasi-static loading under ambient temperature [6]. It is not feasible to model these experiments with MD, because of the computational cost of low strain-rate simulations. For example, for a strain rate of 1 x 10^8 s^{-1}, a single uniaxial tension simulation took about 40 hours on Georgia Tech's Partnership for an Advanced Computing Environment (PACE), using 64 cores and 64 GB RAM. In MD, the response of large systems is typically simulated by applying periodic boundary conditions, which makes it challenging to capture strain localization and brittle failure. For instance, it is well-known that for polymer systems well below the glass transition temperature, MD simulations over-predict strength and do not capture brittle failure [24]. It was also noted that compression strength of polymers increases with the loading rate [30].

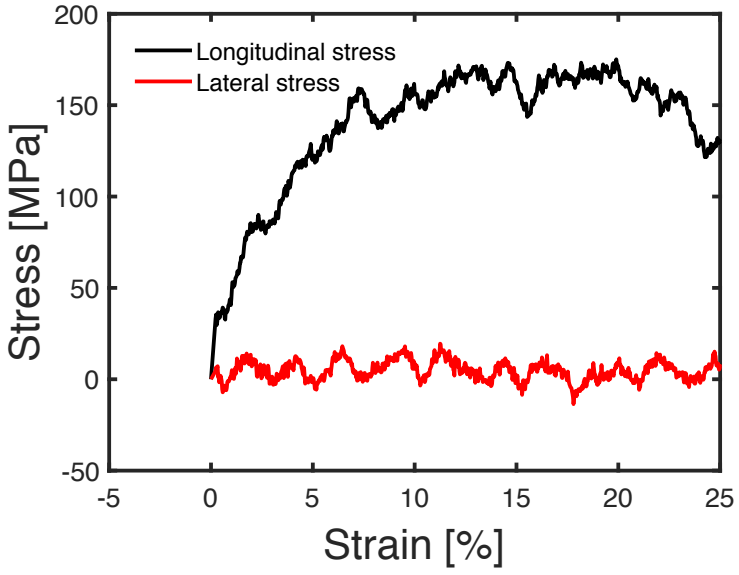

(a)

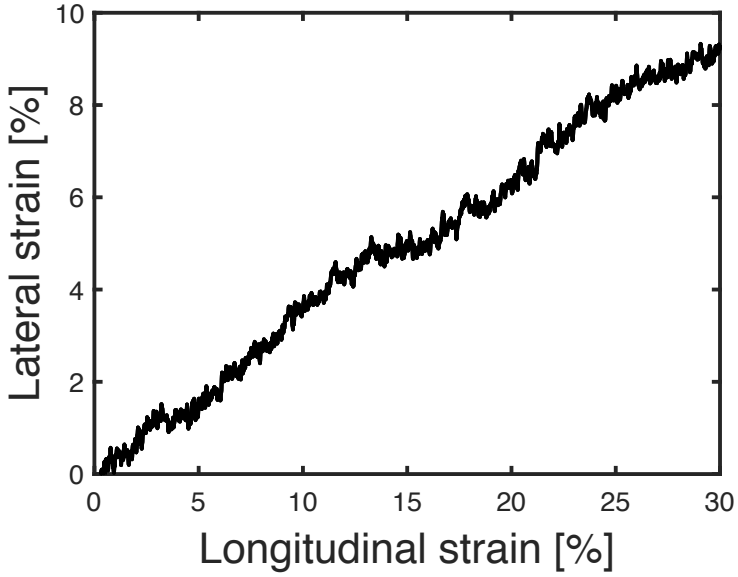

(b)

Figure 5: Simulation of a uniaxial tension test on cross-linked HMWM at $300K$, at atmospheric pressure and using a strain rate of 5 x 10^8 s^{-1}. (a) Stress-strain response (b) Lateral vs. longitudinal strain curve.

We simulated the uniaxial tension test at three different strain rates (1 x $10^8 s^{-1}$; 5 x $10^8 s^{-1}$; 1 x $10^9 s^{-1}$). Figure 6 shows the stress-strain curves that we obtained numerically. We verify that the stress at the yield point increases with the loading strain rate (here, we define yield point as the point where the non-linear behavior initiates). We also note that, in average, when strains are in the range 4 - 7 %, the secant stiffness (Young's modulus) predicted numerically increases with the strain rate. This trend is consistent with the results obtained with MD by other authors (e.g., [24, 30]). In the discussion that follows (Section 4), we use Richeton's model [30] to explain how numerical predictions can be extrapolated to predict the HMWM tensile modulus at lower strain rates. In the following, all the MD simulations are conducted with a loading strain rate of 5 x 10^8 s^{-1}, unless otherwise stated.

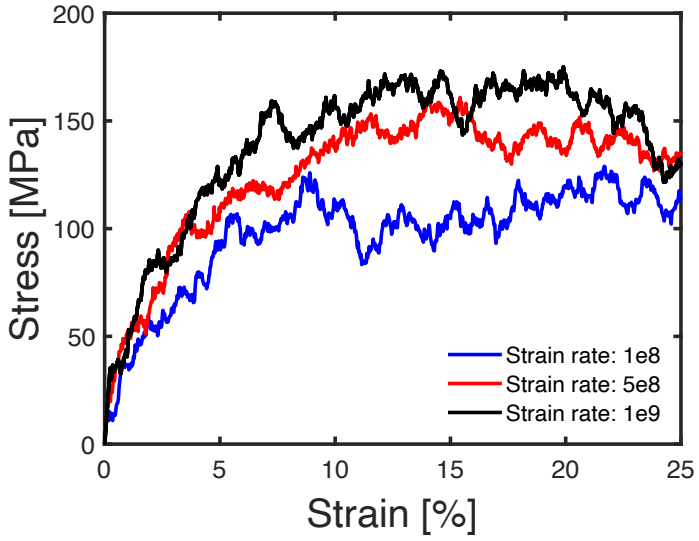

Figure 6: Effect of strain rate on the mechanical behavior of HMWM.

3. Molecular model of the mineral-HMWM interface

3.1. Construction of the MD interface models

We simulated pullout tests on HMWM/concrete interfaces at the molecular scale. Concrete was represented by a layer of either calcite or crystalline silica. The lattices of calcite and silica are shown in Figure 1. Both mineral structures were cleaved in the [0, 0, 1] direction (on the interface side) to build the mineral substrate. The cleaved mineral blocks were generated in an amorphous cell in MAPS. A vacuum cell was added on top. The vacuum cells were then packed with crosslinked HMWM (Figure 2). The dimensions of the simulations cells (W * D * H) were chosen based on previous studies [12, 19], see Table 1. The bi-material HMWM/mineral interfaces are shown in Figure 7.

Table 1: Dimensions of the simulation cells.

Minerals	Number of atoms	W * D * H (Å)
Calcite	9,232	39.92 * 34.12 * 69.14
Silica	9,319	35.58 * 38.46 * 70.44

Geometry optimization and NPT equilibration tests were conducted with the interface models, in a similar way as for the HMWM model presented in Subsection 2.3. The interface debonding tests were simulated by fixing the bottom layer of the mineral substrate and by applying a tensile strain rate at the top of the HMWM layer. The DREIDING force field was applied and the non-bonding forces were calculated with a cutoff distance of 12Å.

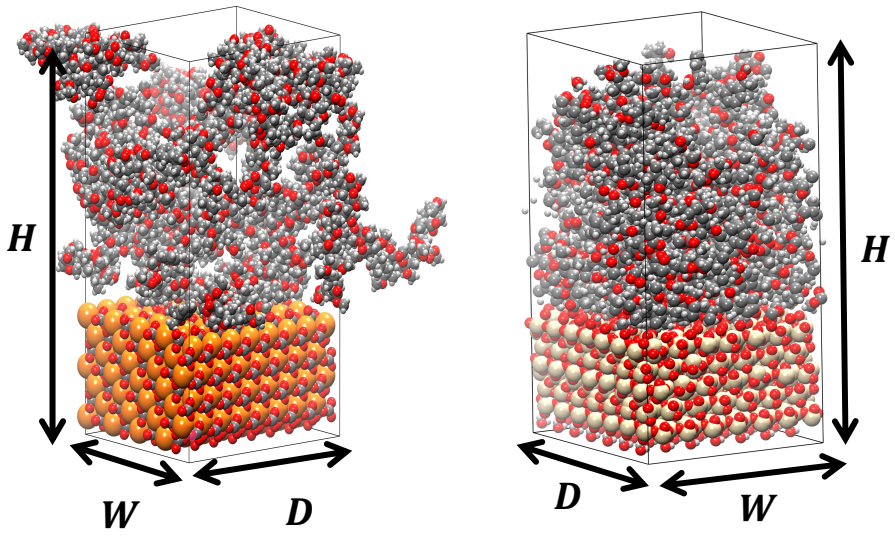

(a) (b)

Figure 7: Molecular interface systems for (a) the calcite-HMWM model and (b) the silica-HMWM model.

3.2. Results of the numerical interface debonding tests

3.2.1. Effect of the mineral substrate

We first compared the results obtained with calcite and with silica for a debonding test conducted at a rate of $5\text{x}10^{8}\text{s}^{-1}$, under a temperature of 300K. A single pullout simulation took about 65 hours on Georgia Tech's Partnership for an Advanced Computing Environment (PACE), using 64 cores and 64 GB RAM. The fluctuations of the simulation results were smoothened using the moving average function implemented in MATLAB. The resulting stress-strain curves are shown in Figure 8. Both calcite and silica interfaces initially present a linear stress-strain response up to the peak stress, which is followed by a significant stress drop, indicating a reduction of HMWM/minerals inter-

actions. After debonding of the HMWM/mineral interface, stress converges to zero. The interfacial strength is higher for the HMWM/silica interface than for the HMWM/calcite interface.

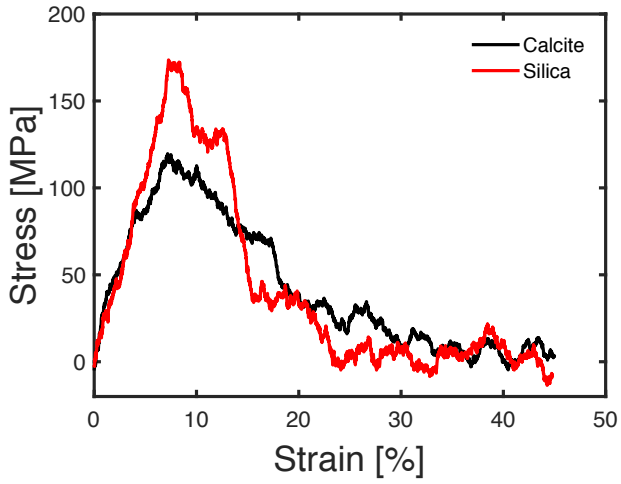

Figure 8: HMWM/mineral interface debonding tests simulated at 300 K, at a rate of $5x10^{8}s^{-1}$, for two different concrete minerals: silica and calcite.

We repeated the debonding tests in the presence of moisture. Starting with the interface model without water molecules, a thin confined layer of 100 water molecules was inserted between the mineral substrate and HMWM, following the method proposed by Y. Gao and collaborators [19]. The interface models with water molecules were then subjected to the same geometry optimization and equilibration procedures as for interface models without water molecules. Stress-strain curves and snapshots of atomic configurations are shown in Figures 9 and 10. Stretching (phase A) is followed by microvoid formation (sequence B-C). Final separation is captured (phase D) and the critical failure plane is found to be at the interface between HMWM and the

mineral for both calcite and silica.

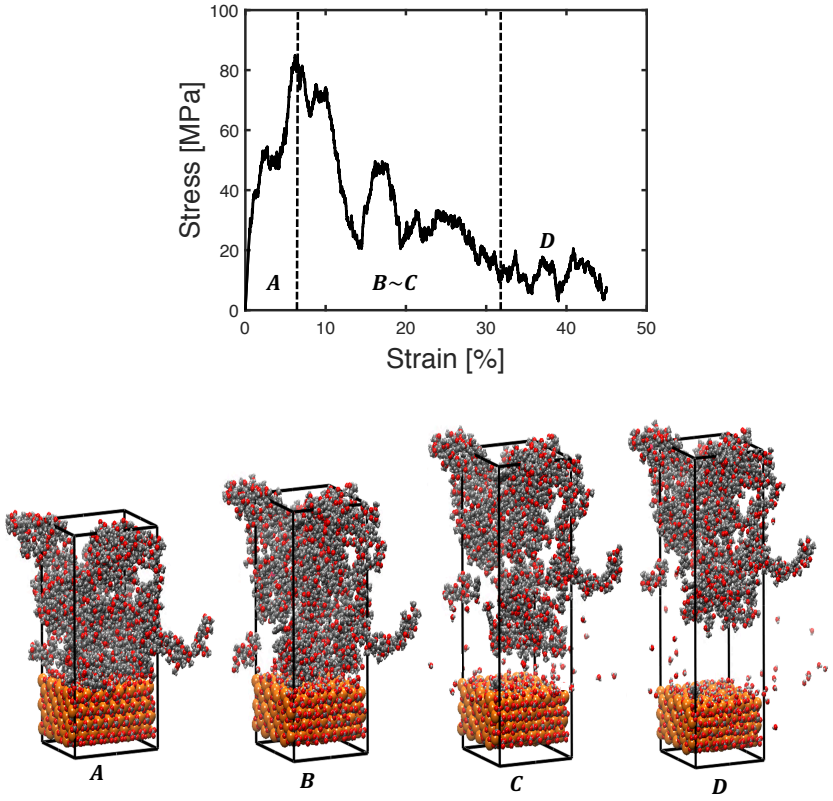

Figure 9: Calcite-water-HMWM interface system during the interface debonding test at a rate of 5x10^{8}s^{-1}, under a temperature of 300K, with 100 water molecules.

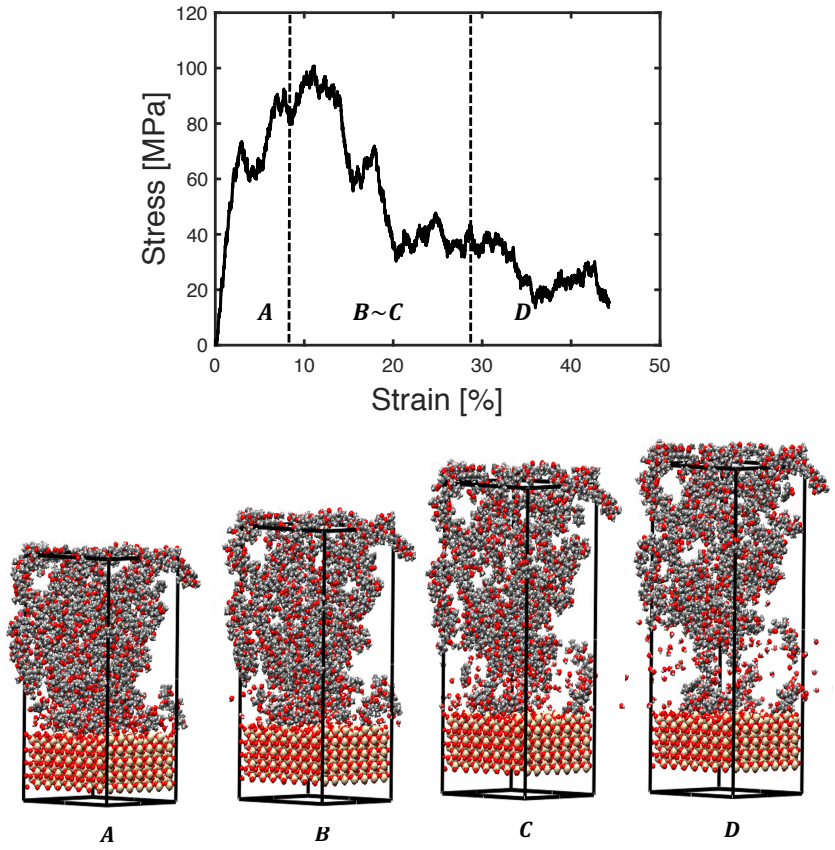

Figure 10: Silica-water-HMWM interface system during the interface debonding test, at a rate of $5x10^8 s^{-1}$, under a temperature of 300K, with 100 water molecules.

3.2.2. Effect of temperature and moisture

We studied the response of the HMWM/water/mineral interface systems at five temperatures (200 K, 250 K, 300 K, 350 K, 400 K). The strain rate was $5x10^8 s^{-1}$ and 100 water molecules were present at the interfaces. The simulation results indicate that the primary separation occurs at the interface between HMWM and the mineral substrate. The deformation of the HMWM bulk does not exhibit any dependence to temperature. Figure 11 shows that the strength of both the HMWM/silica and HMWM/calcite interfaces decreases when temperature increases. For example, for the HMWM/calcite interface system, we note a 16% decrease of interface strength from 200 K to 300 K and a 63% decrease of interface strength between 300 K and 400 K. The dependence of tensile strength to temperature was expected for this range of temperature, since the glass transition temperature is around 407 K.

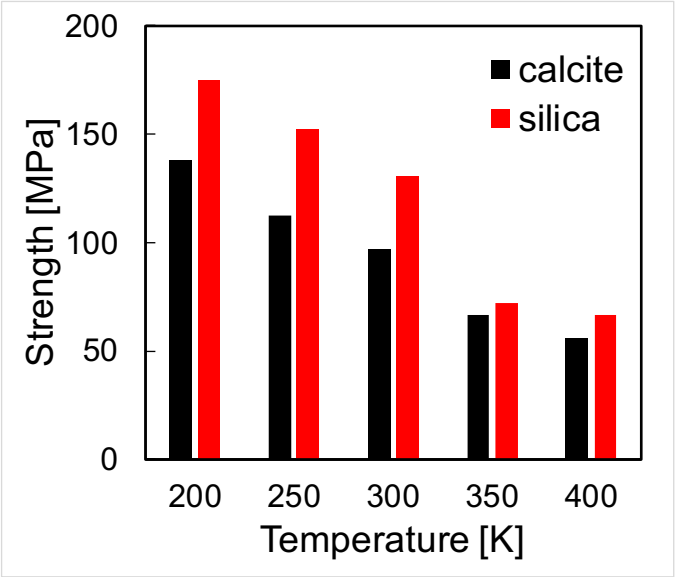

Figure 11: Interface strength predicted by MD under different temperatures.

Interface strength and work of separation were calculated for both substrates during the interface debonding tests performed at 300 K, with and without moisture. Results are presented in Figure 12. The work of separation was calculated as the area of the stress-displacement curve divided by the energy required to separate a unit area of interface. The strength of the silica/HMWM interface is 30 MPa higher than the HMWM/calcite interface, regardless of moisture conditions. In the presence of moisture, interface strength decreases by 32% for the calcite/HMWM interface and by 26% for the silica/HMWM interface. In dry conditions, the work of separation is about $175 mJ/m^2$ for both the calcite and the silica systems. In the presence of moisture, the work of separation is 125.97 mJ/m^2 for the calcite/HMWM interface and $156.69 mJ/m^2$ for the silica/HMWM interface.

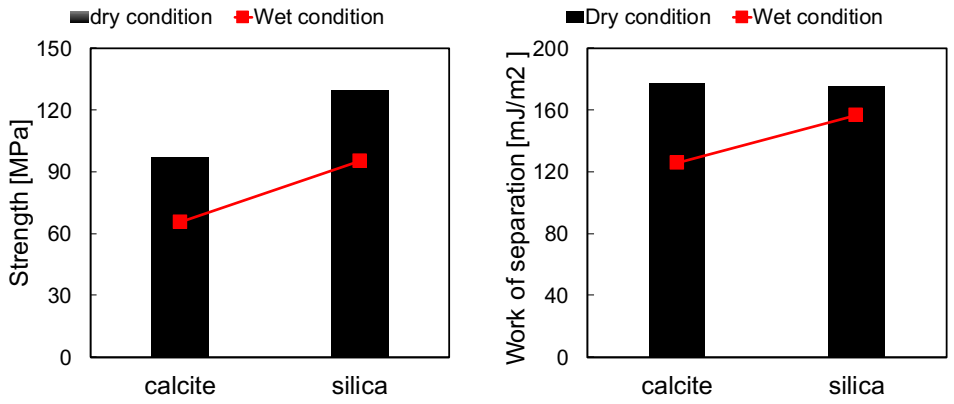

(a) Tensile strength

(b) Work of separation

Figure 12: Interface strength predicted by MD under different moisture conditions.

3.2.3. Effect of strain rate

We simulated the interface debonding test at three strain rates: $10^9 s^{-1}$, $5\times10^8 s^{-1}$, and $1\times10^8 s^{-1}$, under a 300 K temperature. The stress-strain curves obtained for the calcite and silica interface models are shown in Fig 13. The shape of the stress-strain curves and the peak strength are influenced by the strain rate. We note that the peak stress is higher than the peak stress reported in experimental studies [6]. This is because the strain rates used in the MD simulations were way higher than the rates used in the experiments. As explained above, the computational cost of the MD simulations is prohibitive, which does not allow analyzing the sensitivity of our interface model at quasi-static strain rates. In Section 4, we discuss how to overcome this limitation.

The simulation results indicate that for both mineral substrates, the higher the strain rate, the higher the peak strength and the higher the total area of the stress/strain curve. These results are consistent with observations made by previous researchers [17]. We also note that the elastic behavior of the interface systems does not exhibit significant dependency to strain rate.

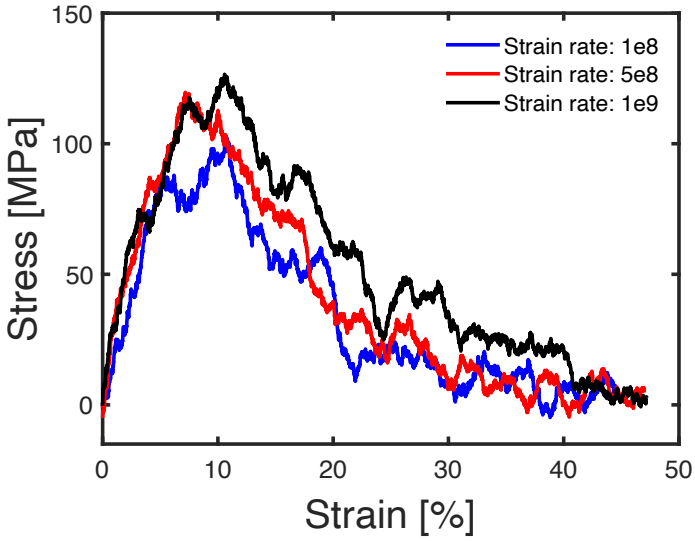

(a) Calcite substrate

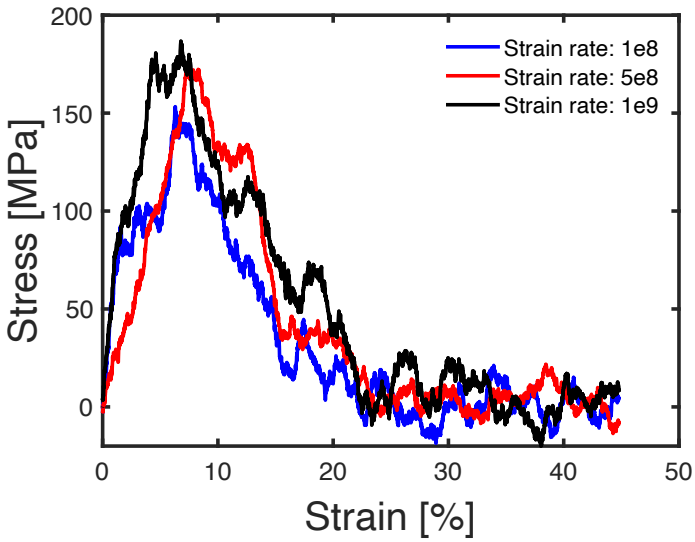

(b) Silica substrate

Figure 13: Effect of strain rate on the mechanical behavior of the HMWM/mineral interface during the interface debonding tests.

4. Discussion

4.1. Interface strength and fracture energy

The stress-strain response predicted in the MD interface tension tests is similar to a cohesive law, which led some authors to use the MD stress-strain curve as a traction-separation law to define a Cohesive Zone Model (CZM) at the metric or submetric scale [13, 12, 11]. Figure 14 illustrates this method. As an example, we fitted an exponential traction-separation law (in red) to the stress-strain response obtained during the interface debonding test conducted with the dry HMWM/silica interface system at a loading rate of $1{\times}10^{8}\mathrm{s}^{-1}$, under a temperature of 300 K and at atmospheric pressure. The

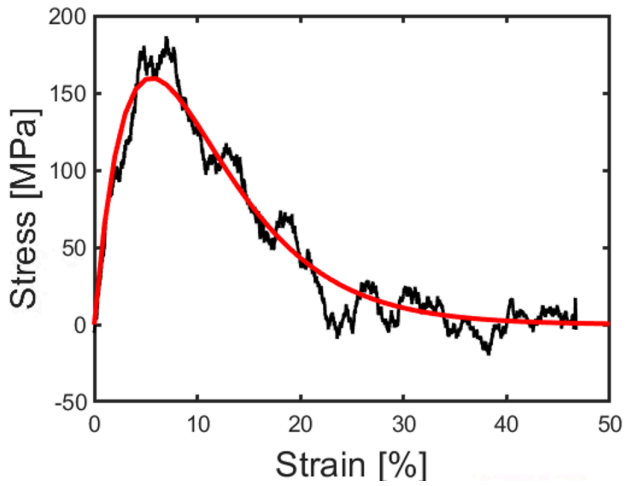

Figure 14: Characterization of interfacial debonding by using an exponential cohesive zone model. Dry HMWM/silica interface loaded at $1{\times}10^{8}\mathrm{s}^{-1}$, under a temperature of 300 K and at atmospheric pressure.

exponential softening curve has the following equation:

$$\sigma = \sigma_c \left(\frac{\varepsilon}{\varepsilon_c}\right) exp\left(1 - \frac{\varepsilon}{\varepsilon_c}\right) \tag{6}$$

where σ_c is the peak stress and ε_c is the critical strain, defined as the strain that is reached when $\sigma = \sigma_c$. After fitting, it is found that the strength of the dry interface is 152.22 MPa and the critical strain is 9%, with an R-square error of 95%. As shown in Figures 9 and 10, the interfacial strength and the critical strain of the HMWM/water/calcite system are 66.81MPa and 7.5% respectively, while the interfacial strength and the critical strain of the HMWM/water/silica system are 86.89MPa and 7.34% respectively. These interfacial strengths are 16 times larger than the interfacial strengths found experimentally [31]. This difference is due to size effects and to strain rate effects. Size effects cannot be avoided and in that sense, we conclude that the stress-strain curve obtained by MD cannot be used as is in a macroscopic CZM model. However, the Richeton's model can be calibrated to extrapolate the MD predictions made at high strain rate to lower strain rates. We calibrate the Richeton's model in the following section.

4.2. MD predictions at low strain rate with phenomenological models

The effects of strain-rate and temperature on the mechanical behavior of composites and polymers were investigated by using the Richeton's model and the Johnson-Cook model's [32, 33, 34, 35]. In this study, we used these two phenomenological models to predict the tensile modulus of HMWM and the strength of the HMWM/concrete interface. Based on the Richeton's model, the elastic modulus of polymers is expressed as [30]:

$$E_y = E_y^{ref}\left(1 + Sln\left(\frac{\dot{\varepsilon}}{\dot{\varepsilon}^{ref}}\right)\right) \tag{7}$$

where E_y and E_y^{ref} are the elastic modulus and the reference elastic modulus under a static loading rate, S is strain rate sensitivity constant, $\dot{\varepsilon}$ and $\dot{\varepsilon}^{ref}$

are the effective plastic strain rate and the reference strain rate.

We calibrated the S parameter to fit the Richeton's model to the MD results of HMWM uniaxial tension tests. For the reference elastic modulus, the tensile modulus of HMWM is 0.28GPa at a tensile strain rate of $0.1s^{-1}$, according to experimental work reported in [6]. We found a good fit between the Richeton's model and the MD results with $S = 0.3428$. The predictions of the Richeton's model, shown with a red dashed line in Figure 15, could be used to predict the values of the tensile modulus under low strain rate if more experimental results were available to check the extrapolation.

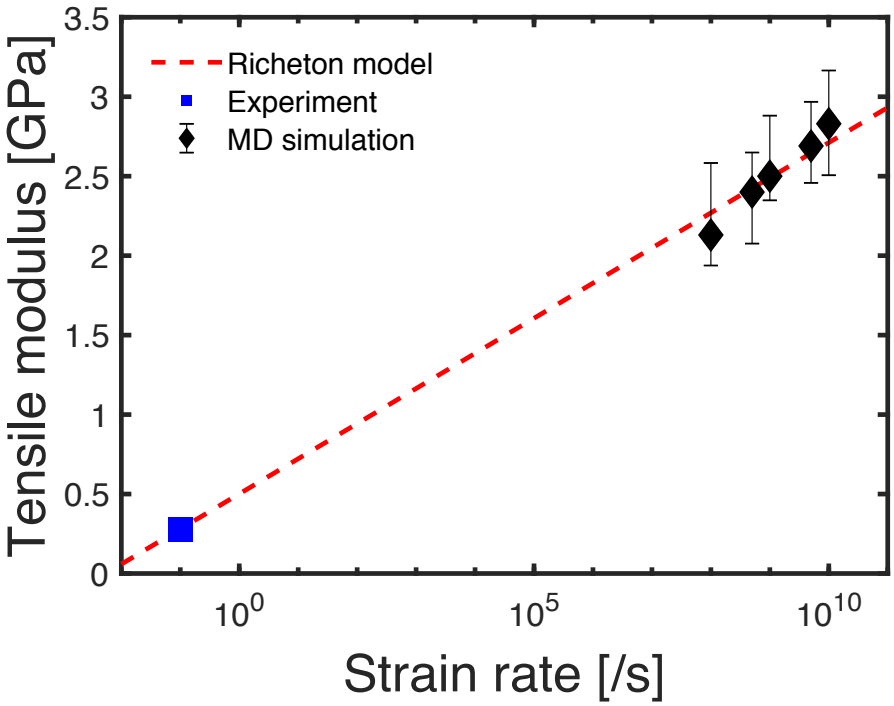

Figure 15: Variation of the tensile modulus of HMWM as a function of strain rate in a uniaxial tension test. Experimental data is used as reference. Blue dot: reference experimental data. Black dots: MD results.

The Johnson-Cook model expresses the dependence of interface tensile strength to the strain rate and to temperature, according to the following equation [36]:

$$\sigma_y = \sigma_y^{ref}\left[1 + Cln\left(\frac{\dot{\varepsilon}}{\dot{\varepsilon}^{ref}}\right)\right]\left[1 - \left(\frac{T - T_{room}}{T_g - T_{room}}\right)^m\right] \quad (8)$$

where σ_y and σ_y^{ref} are the yield strength and the reference yield strength under a static loading rate, C is a strain rate sensitivity constant, T_{room} and T_g are the room temperature and the glass transition temperature, m is a temperature sensitivity parameter. Based on the PCC-SSD bond strength test results reported in the technical datasheet of Transpo company [31], the tensile strength of the HMWM/concrete interface is 4.2MPa at a reference strain rate of $0.1s^{-1}$. We calibrated the values of parameters C and m to match the MD results of interface debonding tests. We found $C = 1.019$ and $m = 0.441$. The predicitons of the Johnson-Cook model, represented by a hyper-surface in Figure 16, could be used to predict the variations of interface tensile strength with temperature and strain rate, if more experimental data was available to check the extrapolation. In general, interfacial strength increases when temperature decreases and when the strain rate increases.

4.3. Contribution of the non-bonded energy to the work of separation of the HMWM/mineral interfaces

Figure 17 presents the evolution of the work of separation, the non-bonding energy and the bonding energy of the HMWM/mineral interfaces during the interface debonding tests simulated by MD. The non-bonding energy E_{nb} and the bonding energy E_b were calculated according to Equation 3. Results show that the work of separation is always almost equal

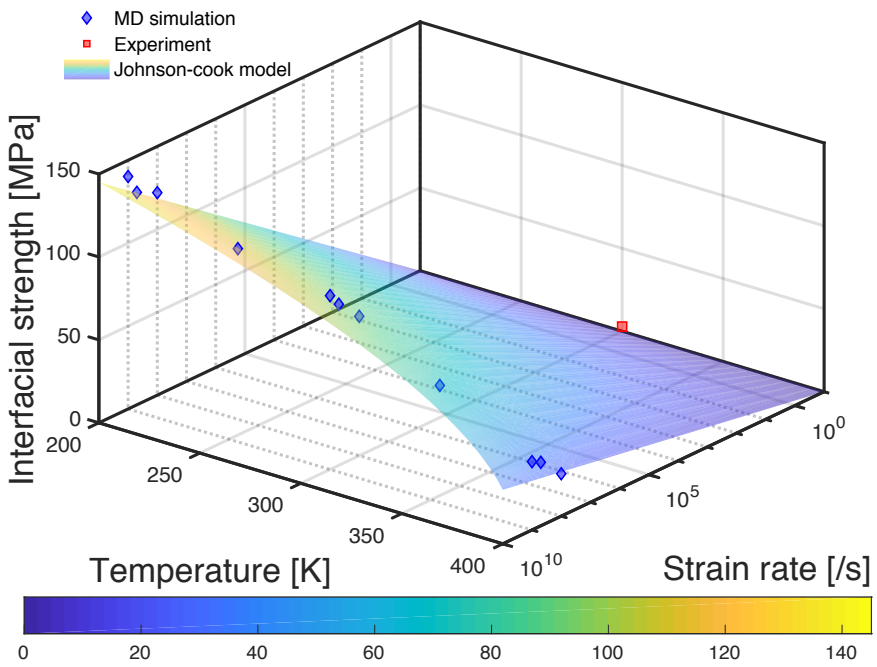

Figure 16: Interfacial strength as a function of strain rate and temperature using Johnson-Cook model for the HMWM/calcite interface model. The red dot is an experimental data point. The blue dots are the data points obtained by MD simulation.

to $E_b + E_{nb}$. We note that the bonding energy oscillates between positive and negative values. This trend was already noted in [37]. Additionally, the contribution of the bonding energy to the work of separation is negligible for the HMWM/silica interfaces. The bonding energy was equal to a fifth of the non-bonding energy for the HMWM/calcite interfaces. For both HMWM/mineral interfaces, van der Waals forces were thus the main forces that resisted debonding. This somewhat surprising result was already highlighted in previous studies, e.g. [17, 12, 19, 11, 37].

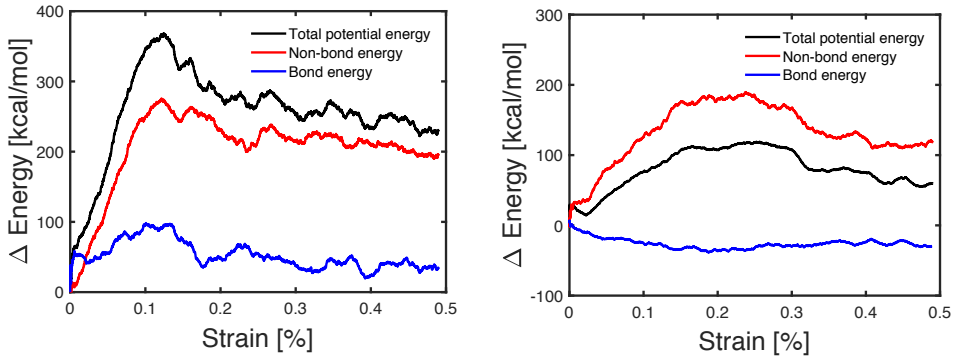

(a) Interface between HMWM/calcite (b) Interface between HMWM/silica

Figure 17: Energy distribution during debonding tests of dry interfaces at 300 K for a strain rate of $5 \times 10^8 s^{-1}$.

5. Conclusions

High Molecular Weight Methacrylate (HMWM) is broadly used as a sealant in the construction industry, to repair narrow cracks in concrete. HMWM is efficient for clogging cracks and preventing the corrosion of steel reinforcements by chloride. However, there is no fundamental understanding on how HMWM changes the mechanical properties of concrete. In this paper, we propose an analysis of the mechanical properties of the HMWM/concrete interface based on Molecular Dynamics (MD). The glass transition temperature and the mass density predicted by the MD model of HMWM are conform to experimental data reported in the literature. Interface models are proposed for two mineral phases widely present in concrete: calcite and silica. The results of the uniaxial tension tests show that all interfaces fail by debonding, at the surface of contact between HMWM and the mineral substrate. Moreover, the interfacial strength decreases in the presence of moisture, under low strain rate, or at high temperature. Silica/HMWM interfaces

are stronger than the calcite/HMWM interfaces. Additionally, MD results show that the work of separation is mostly done by van der Waals forces, which is in agreement with previous studies. Specifically, the non-bonding energy is negligible for the HMWM/silica interfaces and the bonding energy is equal to a fifth of the non-bonding energy for the HMWM/calcite interfaces. We use published experimental data at low strain rate along with our MD results at high strain rate to calibrate the Richeton's model and the Johnson-Cook model. We show that, if more experimental data were available for validation, our MD results could be extrapolated to predict the tensile modulus of HMWM at low strain rate and the HMWM/mineral interfacial strength for a broad range of temperatures and strain rates. MD results confirm that HMWM should be applied on dry surfaces and in concrete exposed to lower temperatures. Furthermore, our MD simulations highlighted an important new finding: HMWM is more likely to last in concrete with high silica contents than in concrete with high calcite contents.

Acknowledgements

Support for this research was provided by the Georgia Department of Transportation, as part of the project entitled "Mechanical integrity and sustainability of pre-stressed concrete bridge girders repaired by epoxy injection" (RP 16-24, RP 17-08 and RP 17-12). Any opinions, findings and conclusions or recommendations expressed in this paper are those of the author(s), and do not necessarily reflect the views of the Georgia Department of Transportation.

References

References

[1] R. E. Weyers, M. M. Sprinkel, Concrete Bridge Protection , Repair , and Re h abilitation Relative to Reinforcement Corrosion : A Methods Application Manual, strategic Edition, National Academy of Sciences, 1993.

[2] S. Soltesz, Crack Sealer Fill Characteristics, Tech. rep., Oregon Department of Transportation (2010).

[3] T. L. Reguianski, The Air Force Institute of Technology, IRE Transactions on Education E-5 (2) (2008) 117–118. doi:10.1109/te.1962.4322266.

[4] V. J. Marks, High Molecular Weight Methacrylate Sealing of a Bridge Deck, Transportation Research Record (1986) 83–88.
URL http://onlinepubs.trb.org/Onlinepubs/trr/1988/1204/1204-012.pdf

[5] A. Rahim, D. Jansen, N. Abo-Shadi, J. Simek, Overview of High-Molecular-Weight Methacrylate for Sealing Cracks in Concrete Bridge Decks, Transportation Research Record: Journal of the Transportation Research Board 2202 (2202) (2010) 77–81. doi:10.3141/2202-10.
URL http://trrjournalonline.trb.org/doi/10.3141/2202-10

[6] D. A. Meggers, Final Report Crack Sealing and Repair of Older Serviceable Bridges Using Polymer Sealers (January) (1998) 130. doi:FHWA-KS-98-4.

[7] O. Coussy, P. J. Monteiro, Poroelastic model for concrete exposed to freezing temperatures, Cement and Concrete Research 38 (1) (2008) 40–48. doi:10.1016/j.cemconres.2007.06.006.

[8] F. Ulm, G. Constantinides, F. H. Heukamp, Is concrete a poromechanics material ?— A multiscale investigation of poroelastic properties Is concrete a poromechanics material ? - A multiscale investigation of poroelastic properties (April 2012) (2016). doi:10.1007/BF02481626.

[9] S. Ghabezloo, J. Sulem, S. Guédon, F. Martineau, J. Saint-marc, Cement and Concrete Research Poromechanical behaviour of hardened cement paste under isotropic loading, Cement and Concrete Research 38 (12) (2008) 1424–1437. doi:10.1016/j.cemconres.2008.06.007.
URL http://dx.doi.org/10.1016/j.cemconres.2008.06.007

[10] C. A. Coronado, M. M. Lopez, Damage approach for the prediction of debonding failure on concrete elements strengthened with FRP, Journal of Composites for Construction 11 (4) (2007) 391–400. doi:10.1061/(ASCE)1090-0268(2007)11:4(391).
URL http://link.aip.org/link/JCCOF2/v11/i4/p391/s1&Agg=doi

[11] W. G. Jiang, Y. Wu, Q. H. Qin, D. S. Li, X. B. Liu, M. F. Fu, A molecular dynamics based cohesive zone model for predicting interfacial properties between graphene coating and aluminum, Computational Materials Science 151 (April) (2018) 117–123. doi:10.1016/j.commatsci.2018.05.008.
URL https://doi.org/10.1016/j.commatsci.2018.05.008

[12] G. Xu, H. Wang, Molecular dynamics study of interfacial mechanical behavior between asphalt binder and mineral aggregate, Construction and Building Materials 121 (2016) 246–254. doi:10.1016/j.conbuildmat.2016.05.167.
URL http://dx.doi.org/10.1016/j.conbuildmat.2016.05.167

[13] A. Sazgar, M. R. Movahhedy, M. Mahnama, S. Sohrabpour, Development of a molecular dynamic based cohesive zone model for prediction of an equivalent material behavior for Al/Al2O3 composite, Materials Science and Engineering A 679 (October 2016) (2017) 116–122. doi:10.1016/j.msea.2016.10.001.
URL http://dx.doi.org/10.1016/j.msea.2016.10.001

[14] C. L. Soles, A. F. Yee, A Discussion of the Molecular Mechanisms of Moisture Transport in Epoxy Resins, Journal of Polymer Science: Part B: Polymer Physics (September) (1999) 792–802.

[15] B. J. Alder, T. E. Wainwright, Studies in molecular dynamics. General method, Journal of chemical physics 31 (2) (1959) 459. arXiv:1.1730376., doi:10.1063/1.1730376.
URL http://link.aip.org/link/?JCPSA6/31/459/1

[16] H. R. Sasse, M. Fiebrich, Bonding of polymer materials to concrete, Matériaux et Constructions 16 (4) (1983) 293–301. doi:10.1007/BF02473695.

[17] S. Yang, F. Gao, J. Qu, A molecular dynamics study of tensile strength between a highly-crosslinked epoxy molding compound and a cop-

per substrate, Polymer (United Kingdom) 54 (18) (2013) 5064–5074. doi:10.1016/j.polymer.2013.07.019.
URL http://dx.doi.org/10.1016/j.polymer.2013.07.019

[18] K. Min, Y. Kim, S. Goyal, S. H. Lee, M. McKenzie, H. Park, E. S. Savoy, A. R. Rammohan, J. C. Mauro, H. Kim, K. Chae, H. S. Lee, J. Shin, E. Cho, Interfacial adhesion behavior of polyimides on silica glass: A molecular dynamics study, Polymer (United Kingdom) 98 (2016) 1–10. doi:10.1016/j.polymer.2016.06.017.
URL http://dx.doi.org/10.1016/j.polymer.2016.06.017

[19] Y. Gao, Y. Zhang, F. Gu, T. Xu, H. Wang, Impact of minerals and water on bitumen-mineral adhesion and debonding behaviours using molecular dynamics simulations, Construction and Building Materials 171 (2018) 214–222. doi:10.1016/j.conbuildmat.2018.03.136.
URL https://doi.org/10.1016/j.conbuildmat.2018.03.136

[20] D. Lau, W. Jian, Z. Yu, D. Hui, Nano-engineering of construction materials using molecular dynamics simulations: Prospects and challenges, Composites Part B: Engineering 143 (March) (2018) 282–291. doi:10.1016/j.compositesb.2018.01.014.
URL https://doi.org/10.1016/j.compositesb.2018.01.014

[21] Y. L. Yaphary, Z. Yu, R. H. W. Lam, D. Hui, D. Lau, Molecular dynamics simulations on adhesion of epoxy-silica interface in salt environment, Composites Part B: Engineering 131 (2017) 165–172. doi:10.1016/j.compositesb.2017.07.038.
URL http://linkinghub.elsevier.com/retrieve/pii/S1359836817308806

[22] D. Fan, S. Yang, Mechanical properties of C-S-H globules and interfaces by molecular dynamics simulation, Construction and Building Materials 176 (2018) 573–582. doi:10.1016/j.conbuildmat.2018.05.085.
URL https://doi.org/10.1016/j.conbuildmat.2018.05.085

[23] A. Bandyopadhyay, P. K. Valavala, G. M. Odegard, Atomistic Modelling of Crosslinked Epoxy Polymer, Structure (17th ICCM Conference Proceedings) (2009).

[24] C. Li, A. Strachan, Molecular simulations of crosslinking process of thermosetting polymers, Polymer 51 (25) (2010) 6058–6070. doi:10.1016/j.polymer.2010.10.033.
URL http://dx.doi.org/10.1016/j.polymer.2010.10.033

[25] M. Yang, P. Qiao, D. I. McLean, B. Khaleghi, Effects of overheight truck impacts on intermediate diaphragms in prestressed concrete bridge girders, PCI Journal 55 (1) (2010) 58–78.
URL http://www.scopus.com/inward/record.url?eid=2-s2.0-76649095360&partnerID=

[26] D. Hossain, M. A. Tschopp, D. K. Ward, J. L. Bouvard, P. Wang, M. F. Horstemeyer, Molecular dynamics simulations of deformation mechanisms of amorphous polyethylene, Polymer 51 (25) (2010) 6071–6083. doi:10.1016/j.polymer.2010.10.009.
URL http://dx.doi.org/10.1016/j.polymer.2010.10.009

[27] L.-h. Tam, D. Lau, A molecular dynamics investigation on the cross-linking and physical properties of epoxy-based materials, RSC Adv.

4 (62) (2014) 33074–33081. doi:10.1039/C4RA04298K.
URL http://xlink.rsc.org/?DOI=C4RA04298K

[28] S. Plimpton, Fast parallel algorithms for short-range molecular dynamics (1995). doi:10.1006/jcph.1995.1039.

[29] K. Yamamoto, H. Tanaka, M. Sakaguchi, S. Shimada, Well-defined poly (methyl methacrylate) grafted to polyethylene with reverse atom transfer radical polymerization initiated by peroxides, Polymer 44 (2003) 7661–7669. doi:10.1016/j.polymer.2003.10.006.

[30] J. Richeton, S. Ahzi, Modeling and validation of the large deformation inelastic response of amorphous polymers over a wide range of temperatures and strain rates, International Journal of Solids and Structures 44 (2007) 7938–7954. doi:10.1016/j.ijsolstr.2007.05.018.

[31] Transpo, Technical Data Sheet-High Molecular Weight Methacrylate (HMWM) Crack Sealer Sealate® (T-70-10 and T-70 MX-30) (2017).
URL https://www.transpo.com/roads-highways/materials/concrete-crack-sealers/s

[32] S. Shadlou, B. Ahmadi-Moghadam, F. Taheri, The effect of strain-rate on the tensile and compressive behavior of graphene reinforced epoxy/nanocomposites, Materials and Design 59 (2014) 439–477. doi:10.1016/j.matdes.2014.03.020.
URL http://dx.doi.org/10.1016/j.matdes.2014.03.020

[33] T. J. Holmquist, J. Bradley, A. Dwivedi, D. Casem, The response of polymethyl methacrylate (PMMA) subjected to large strains, high strain rates, high pressures, a range in temperatures, and variations in

the intermediate principal stress, European Physical Journal: Special Topics 225 (2) (2016) 343–354. doi:10.1140/epjst/e2016-02636-5.

[34] H. Wu, X. Li, Q. Mei, J. Chen, G. Wu, Flow behavior of diffusion bonding interface of Ti6Al4V alloy over a wide range of strain rates, Materials Science and Engineering A 761 (June) (2019) 138067. doi:10.1016/j.msea.2019.138067.
URL https://doi.org/10.1016/j.msea.2019.138067

[35] Z. Jia, G. Yuan, H. L. Ma, D. Hui, K. T. Lau, Tensile properties of a polymer-based adhesive at low temperature with different strain rates, Composites Part B: Engineering 87 (2016) 227–232. doi:10.1016/j.compositesb.2015.10.013.
URL http://dx.doi.org/10.1016/j.compositesb.2015.10.013

[36] G. R. Johnson, W. H. Cook, Fracture characteristics of three metals subjected to various strains, strain rates, temperatures and pressures, Engineering Fracture Mechanics 21 (1) (1985) 31–48. doi:10.1016/0013-7944(85)90052-9.

[37] X. Zhuang, Molecular Dynamics Study of an Amorphous Polyethylene / Silica Interface with Shear Tests, Materials 11 (929) (2018) 14. doi:10.3390/ma11060929.